American Mineralogist, Volume 99, pages 1746–1754, 2014

Bioreduction of biotite and chlorite by a *Shewanella* species† 🔓

Diana R. Brookshaw[1,*], Jonathan R. Lloyd[1], David J. Vaughan[1] and Richard A.D. Pattrick[1]

[1]Williamson Research Centre for Molecular Environmental Science, School of Earth, Atmospheric and Environmental Sciences, University of Manchester, Manchester, M13 9PL, U.K.

Abstract

The interactions between the Fe(III)-reducing bacterium *Shewanella oneidensis* MR-1 and the phyllosilicate minerals biotite and chlorite have been studied. In washed, non-growing cell suspensions, *S. oneidensis* MR-1 was able to mediate the reduction of Fe(III) in biotite and chlorite in the presence and absence of an artificial electron shuttle, and to reduce as much as 36% of the starting Fe(III) in biotite, and 21% in chlorite. This is predominantly a solid-state reaction, as no significant dissolution or change in morphology was observed after microbial reduction. In growing-cell experiments, with Fe(III) as the only electron acceptor, bacterial biomass increased over eight weeks of incubation. Combining the results of (weak acid-extractable) iron characterization by ferrozine assay and bulk solid iron mineral characterization using Mössbauer spectroscopy, has led to the development of a possible mechanism of reduction of Fe(III) in the bulk of the mineral. Long-distance electron transfer between M2 sites along octahedral layers may facilitate the reduction of the bulk mineral. To our knowledge, this is the first study to demonstrate microbially mediated reduction of Fe(III) within biotite, and show the ability of *S. oneidensis* MR-1 to conserve energy for growth from this reduction.

Keywords: Phyllosilicates, trioctahedral mica, iron-reducing bacteria, remediation

Introduction

Microorganisms including bacteria and archaea are widespread in the Earth's surface environment and play a major role in element cycling in the shallow subsurface and bacterially driven redox cycling of iron has the potential to alter the structure (Kim et al. 2004; Kostka et al. 1999) and reactivity of minerals. This can affect contaminant transport and precipitation dynamics (Bishop et al. 2011; Zhang et al. 2011). Therefore an understanding of the effect that microbial Fe(III) reduction has on the structure of minerals, and thus the role minerals play in microbial respiration and ecology, is essential for long-term predictions of mineral behavior in the subsurface.

It is well known that specialist bacteria can reduce ferric iron [Fe(III)] associated with Fe(III) oxides (Cutting et al. 2009; Lovley and Phillips 1988; Roden and Zachara 1996) and clays including smectite (Dong et al. 2003a; Kostka et al. 1996), illite (Dong et al. 2003b; Seabaugh et al. 2006), and montmorillonite (Jaisi et al. 2007). The rate and extent of reduction of Fe(III) oxides relates to mineral surface area (Roden and Zachara 1996), crystallinity (Cutting et al. 2009) and the amount of biogenic Fe(II) adsorbed to the mineral surface (Roden and Urrutia 2002; Roden and Zachara 1996). These factors may also affect the availability of Fe(III) in phyllosilicates for microbial reduction (Dong et al. 2009; Jaisi et al. 2007).

Microbial reduction of Fe(III) can lead to the dissolution of the mineral as the reduced iron is solubilized; for example, in the Fe hydroxyoxides and, to a lesser extent, clay minerals such as nontronite (Dong et al. 2003a). New mineral phases such as illite can also be produced by the microbial reduction of smectite (Kim et al. 2004) or nontronite (Jaisi et al. 2011). Reduction of some phyllosilicates, such as smectite, is associated with a solid-state change in the oxidation state of Fe(III) to Fe(II) (Stucki et al. 1984); in this case, the layers of linked SiO_4 tetrahedra that sandwich the Fe(III)-containing octahedral layer may stabilize the overall mineral structure. This "structural" Fe(III) reduction reaction may be limited either to the site of the reduction, such as an edge site where the octahedral layer iron is exposed, or limited by the coordination of the Fe(III) with preferential reduction of Fe(III) in tetrahedral sites, as observed in nontronite (Jaisi et al. 2005). Clay minerals can also play a role in microbial ecology; for example, the Fe(III)-reducing bacterium *Shewanella oneidensis* MR-1 has been shown to reduce structural iron in smectite and to conserve energy for growth from this process (Kostka et al. 2002).

The wide distribution of phyllosilicates and their reactivity makes them the key reactive components in many Earth surface environments. Much research has concentrated on this group of minerals as they may control contaminant behavior (Dong 2012; Dong et al. 2009). They are also the major iron-bearing phases in subsurface sediments. The interactions between subsurface bacteria and some clays such as smectite are relatively well characterized. However, despite their abundance in many near-surface environments and their potential importance in contaminant retardation (Baik et al. 2010; McKinley et al. 2001), the microbial reduction of biotite and chlorite has not been as well studied as for other phyllosilicates.

* Present address: Williamson Building, SEAES, University of Manchester, Oxford Road, Manchester, M13 9PL, U.K. E-mail: diana.brookshaw@postgrad.manchester.ac.uk

Biotite mica {general formula: $[K(Mg,Fe)_2(AlSi_3O_{10})(OH)_2]$} is the main Fe-bearing mineral in granitic rocks and many crystalline gneisses and is also an important phase in near-surface environments; including, for instance, at the Hanford Nuclear Reservation, Washington State (U.S.A.). Chlorite {general formula: $(Mg,Fe)_5Al[(OH)_8(AlSi_3O_{10})]$} is an alteration product of other ferromagnesian minerals including biotite (Eggleton and Banfield 1985) and is found in altered basic and intermediate igneous rocks, in low-grade metamorphic rocks and as a detrital or diagenetic component in a range of soils and sediments. Both are 2:1 phyllosilicate minerals and have an octahedrally coordinated layer of Mg and Fe ions between sheets of linked SiO_4 tetrahedra. In biotite, these layers are held together by interlayer K^+ cations, whereas in chlorite, the interlayers contain a Mg-rich brucite-like interlayer (which may also contain Fe). Both of these phyllosilicates can contain both Fe(II) and Fe(III) iron in octahedral coordination.

Geomicrobiological studies of these phyllosilicates have concentrated on their weathering. Abiotic dissolution studies suggest that biotite is an important source of potassium in soils. Plants, fungi (Balogh-Brunstad et al. 2008) or lichens (Barker and Banfield 1996) can extract K or other elements from biotite, and may cause its alteration to vermiculite. The observed loss of cations from the mineral can be correlated with the release of organic acids (Balogh-Brunstad et al. 2008; Barker et al. 1998) and the acid dissolution of biotite has been shown to be incongruent. Microbially mediated weathering also causes preferential loss of cations from the interlayers and octahedral sheets of biotite, with the tetrahedral sheet remaining relatively unreactive (Hopf et al. 2009). These weathering studies were carried out under aerobic conditions, despite anaerobic conditions being prevalent at depth.

The dissolution and weathering behavior of chlorite in systems without microorganisms has been studied (Brandt et al. 2003; Kameda et al. 2009; Krawczyk-Barsch et al. 2004). In addition, recent studies demonstrated the ability of Fe(III)-reducing bacteria to enzymatically reduce the ferric iron associated with this mineral (Bishop et al. 2011; Jaisi et al. 2007; Zhang et al. 2011). However, the availability of Fe(III) within biotite, the mechanism of reduction of both biotite and chlorite, and the effect of such reduction on the minerals, remain poorly characterized. In this study, we investigate: (1) the ability of the "model" Fe(III) reducing bacterium *S. oneidensis* MR-1 to reduce Fe(III) associated with biotite or chlorite, both directly and in the presence of an artificial electron shuttle and humic compound analog (AQDS); (2) the impact of microbial reduction on the physical structure and chemistry of biotite and chlorite; and (3) the ability of *S. oneidensis* MR-1 to conserve energy from the reduction of Fe(III) in biotite.

METHOD

Mineral preparation

The biotite and chlorite used in this study were obtained from the Excalibur Mineral Company, New York. The biotite was originally sourced from Silver Crater Mine, Cardiff, Ontario, Canada, and the chlorite from Michigamme Michigan, U.S.A. Their mineral structures were confirmed by powder X-ray diffraction (XRD, performed using a Philips PW 1730 and Bruker D8Advance diffractometer fitted with Göbel mirror, using Cu$K\alpha$ radiation scanning over a 2θ range of 5 to 70° with a step size of 0.02° and counting time of 2 s) and their chemical formulas were calculated based on electron probe microanalysis (EPMA) results (using a CAMECA SX100 instrument operating at 20 kV accelerating voltage and 20 nA beam current and silicate and metal standards).

The biotite was finely powdered and sieved and the 180 to 500 μm fraction extracted for use in the experiments, although this size fraction may have contained a minor amount of biotite flakes with diameter of <180 μm. The powdered mineral was stored in air-tight containers at room temperature until used in experiments.

The chlorite used was a retrograde metamorphic product in samples comprising garnet porphyroblasts (up to 8 cm in size) surrounded by chlorite, as well as some smaller garnet inclusions and minor amounts of magnetite. The chlorite was extracted from the rock by careful abrasion and hand picking, and the resulting powder was sieved through a 100 μm sieve. The chlorite produced a very fine powder and the sieving allowed the removal of garnet fragments (typically larger than 100 μm). The magnetite fraction could not be separated magnetically from the chlorite powder but these impurities in the chlorite were below the detection limit of XRD analysis, which showed the samples to be a monomineralic clinochlore.

The surface areas of the samples were determined by Brunauer-Emmett-Teller (BET) analysis using N_2 gas adsorption. The relative proportions of Fe(III) and Fe(II) in the bulk mineral were determined by Mössbauer spectroscopy.

Bacterial cultures

Shewanella oneidensis MR-1 was obtained from the University of Manchester Geomicrobiology Group culture collection. The bacterium was grown using standard aseptic techniques. Anerobically grown cells were harvested at late log phase via centrifugation for inoculation of further experiments (further details of culturing and harvesting protocols are included in the supplementary information[1]).

Resting cell experiments

Aliquots of the washed cell suspensions were added via a degassed syringe to sealed bottles containing: anaerobic 30 mM $NaHCO_3$ buffer with 80% N_2:20% CO_2 headspace (pH 7); mineral (either biotite or chlorite) in a 1:40 solid to solution ratio by weight; and 10 mM lactate as an electron donor [the mineral-associated Fe(III) acting as the sole electron acceptor]. In specific experiments 10 μM of anthraquinone-2,6-disulfonate (AQDS) was added as an electron shuttle. Mineral-solution/slurry samples for analyses were extracted from each experimental bottle at selected time intervals via syringe. The concentration of soluble Fe(II) was analyzed in aliquots of the supernatant by ICP-AES (see below). Any remaining supernatant was removed under a 95%N_2:5%H_2 atmosphere in a glove box after 28 days of reaction, and the mineral residue was dried and retained for analysis by Mössbauer spectroscopy.

Growing cell experiments

Harvested and washed bacteria were also suspended in bottles where the solution comprised a modified version of the *Shewanella* minimal growth medium [SMM, von Canstein et al (2008), and see supplemental information[1]]. Here, biotite was supplied as large flakes (1–2 cm in diameter) in a 1:40 solid to solution ratio by weight. The growth medium was modified by exclusion of fumarate, so that the only electron acceptor that could be used for conserving energy for growth was biotite-associated Fe(III). The cultures were incubated for up to eight weeks. Sampling was done sacrificially, and the bacteria fixed immediately with formalin (in a concentration giving the equivalent of 2% final concentration of formaldehyde) for fluorescence imaging using Acridine orange (see supplemental information[1]). The fixed samples were kept at a temperature of 4 °C prior to further analysis.

ICP-AES analysis

At each time point, samples were centrifuged and the supernatant separated for analysis of the concentration of Fe in aqueous solution. Weak acid extraction (in 0.5 N HCl for 1 h) of the bioreduced solids was performed, and aliquots of the supernatant were analyzed for major cations (Fe, Al, Si, Mg, Mn, K). These aqueous cation concentrations were quantified by ICP-AES analysis. Aliquots of 0.5 mL of sample were acidified with 2% HNO_3 to a final volume of 5 mL. The analyses were performed using a Perkin-Elmer Optiman 5300 dual view ICP-AES unit.

[1] Deposit item AM-14-801, Supplementary Figures 1–3. Deposit items are stored on the MSA web site and available via the *American Mineralogist* Table of Contents. Find the article in the table of contents at GSW (ammin.geoscienceworld.org) or MSA www.minsocam.org), and then click on the deposit link.

Ferrozine assay

Aliquots of the slurry were used for determination of the weak acid-extractable Fe speciation [Fe(II) and total dissolved Fe] by ferrozine assay (Lovley and Phillips 1987). This method does not extract all structural Fe in silicates, but is used to understand the relative change in the weak acid-extractable fraction of Fe within biotite and chlorite. A slurry sample was reacted with 0.5 N HCl for 1 h. An aliquot of the acid-extracted sample was added to the ferrozine solution, filtered through a 0.22 μm filter and the absorbance at 562 nm recorded (giving a measurement of the Fe(II) in the sample by reference to an appropriate standard curve). Then, an excess of hydroxylamine hydrochloride solution was added to each sample extraction and allowed to react for a further 1 h and measurement step repeated to give the total dissolved Fe in the sample. Fe(II) was converted to a percentage of the total acid-extractable iron, thus normalizing for variations between samples due to the differences in amount of solid extracted from each sample.

Mössbauer spectroscopy

In an anaerobic glove box, dry mineral residues from the control (non-inoculated) and fully bioreduced experiments were mounted on a layer of aluminized polyethylene terephthalate (PETP) with one layer of 0.5 mm clear PETP holding the sample, and a capping layer of 0.075 mm PETP sealed with an epoxy resin to contain the powder anaerobically. Transmission ^{57}Fe Mössbauer spectra were collected at room temperature (~22 °C) using a FAST ComTec 1024-multi-channel analyzer system (γ-ray source: Co-57, 25 mCi). The spectra were fitted using Lorentzian line shapes with Recoil software (version 1.05). Spectra were calibrated with reference to metallic Fe foil.

Environmental scanning electron microscopy

Droplets of bioreduced and non-inoculated mineral slurry from the resting cell experiments were placed directly onto an adhesive carbon pad attached to a sample stub and dried in air. The samples were imaged under low vacuum conditions using an environmental scanning electron microscope (Philips XL30 ESEM-FEG) employing a beam potential of between 10 and 20 kV; elemental analysis, where necessary, was obtained using energy-dispersive X-ray spectrometry (EDAX).

Atomic force microscopy

For imaging by atomic force microscopy (AFM), mineral flakes with microbial biomass were extracted from fixed experimental bottles and dried in air. The dried mineral flakes were placed on carbon stubs and imaged by atomic force microscopy using a Nanoscope III instrument with 10 × 10 μm scanner used in tapping mode. The data collected were analyzed with Nanoscope III software (Veeco instruments). All measurements were based on data recorded with height images.

RESULTS

Mineral characterization

The structures and chemistries of both minerals were characterized prior to their use in experiments with bacteria. No secondary minerals or inclusions were detected in the biotite powder by XRD. Electron probe microanalysis showed that it was iron-rich (17.1 ± 0.1 wt% Fe, Table 1) and had a chemical formula of

$$K_{0.90}Na_{0.06}[Mg_{1.51}Fe(II)_{0.96}Fe(III)_{0.14}Ti_{0.13}Mn_{0.03}](Al_{0.98}Si_3O_8)(OH,F)_2.$$

The chlorite was an Fe-rich clinochlore, with chemical formula

$$[Mg_{0.93}Fe(II)_{3.3}Fe(III)_{0.38}Ti_{0.01}Mn_{0.02}]Al_{1.31}[(OH)_8(Al_{1.4}Si_{2.6}O_{10})].$$

TABLE 1. Summary of mineral characteristics

Mineral	Size (μm)	Surface area[a] (m^2/g)	Iron content (wt%)[b]	Fe(III) % of the Total Fe[c]
Biotite	180–500	9.02	16.4–17.5	12.6
Chlorite	<100	6.43	37.6–39	10.4

[a] Determined by BET analysis.
[b] wt% = determined by electron microprobe analysis (EPMA).
[c] Determined by Mössbauer spectroscopy.

This chlorite composition was similar to that of the chlorite "CCa-2" (Brandt et al. 2003), used in studies of microbial reduction by other workers (Jaisi et al. 2007; Zhang et al. 2011). The chlorite used in the present study contained 38.4 ± 1 wt% Fe (see Table 1). Approximately 12.6% of the Fe in the biotite (~0.14 atoms per formula unit) and 10.4% of the Fe in the chlorite (~0.38 atoms per formula unit) were determined to be Fe(III) from the Mössbauer spectra of the fresh minerals (see below). For the samples used in this study, the two minerals had similar surface areas (biotite: 9.02 m^2/g, chlorite: 6.43 m^2/g).

Microbial reduction

In non-inoculated treatments of both minerals the proportion of acid-extractable Fe(II) as a percentage of the total acid-extractable iron remained stable over the course of the experiment (see Figs. 1a and 1b), but in treatments with bacteria, a large increase in acid-extractable Fe(II) showed that bioreduction had occurred. In fact, *S. oneidensis* MR-1 was able to reduce fully the acid-extractable Fe(III) in biotite with acid-extractable Fe(II) percent in those experiments reaching 99.7 ± 3.6% after 3 days. In the presence of AQDS the microbial reduction proceeded at a more rapid rate, with Fe(II) reaching 98.4 ± 2.3% of the total acid-extractable Fe only 24 h after inoculation with bacteria, and remaining stable thereafter.

Maximum microbial reduction of chlorite was also achieved in approximately three days (showing a similar rate of reduction to that observed by Bishop et al. 2011). However, unlike in experiments with biotite, reduction was incomplete; acid-extractable Fe(II) was 89.4 ± 2.1%. As with biotite, the rate of reduction was enhanced by the addition of AQDS. However, the addition of the electron shuttle did not significantly enhance the extent of reduction of this mineral [with maximum Fe(II) reached being 91.7 ± 1.5% of the total acid-extractable iron], indicating that some of the weak-acid-extractable Fe(III) in chlorite was recalcitrant to microbial reduction.

The majority of the bioreduction-generated Fe(II) is likely to remain associated with the mineral (as a sorbed or edge-complexed fraction, or as bulk mineral structural Fe). However, microbial reduction also stimulated a release of Fe(II) into solution. A small amount of Fe(II), on average 5.0 ± 0.4 μg/L for biotite and 17.6 ± 3.8 μg/L for chlorite, was found to be soluble in abiotic experiments, and its concentration remained relatively stable throughout the experiment (Figs. 1c and 1d). In contrast, the $Fe(II)_{aq}$ concentration increased significantly in all treatments with *S. oneidensis* MR-1. Without an artificial electron shuttle, the maximum $Fe(II)_{aq}$ in experiments with biotite (41.8 ± 4.1 μg/L) was recorded one week after inoculation. The rate of reduction of chlorite was lower, and $Fe(II)_{aq}$ reached a maximum 14 days after inoculation (113.4 ± 1.0 μg/L). In experiments with AQDS, the maximum $Fe(II)_{aq}$ was recorded earlier than in the equivalent experiments without AQDS (1 day and 7 days for biotite and chlorite, respectively).

The iron speciation and coordination environments within the bulk mineral were determined by Mössbauer spectroscopy. The biotite spectrum was typical for this mineral (Dyar 1993; Rancourt et al. 1992) and had a prominent doublet with a large quadrupole splitting [representing the Fe(II) contribution], and a small shoulder indicating a doublet at lower isomer shift

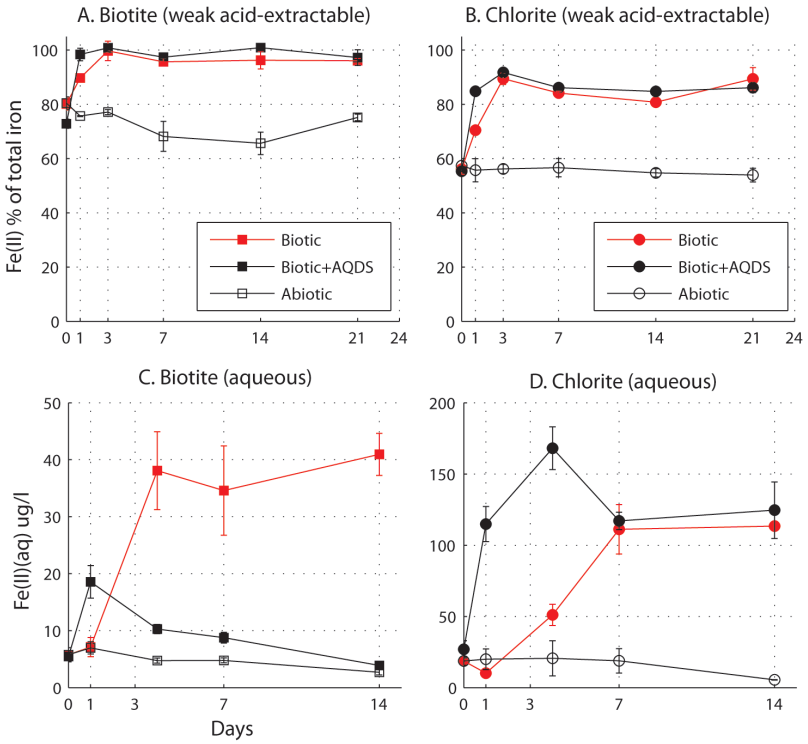

FIGURE 1. Microbial reduction of Fe(III) in biotite and chlorite (as the figures and text list biotite first and chlorite second). The Fe(II) percentage of the total iron in the supernatant and acid-extractable fractions: (**a**) biotite (weak acod-extractable); (**b**) chlorite (weak acid-extractable); (**c**) biotite (aqueous); and (**d**) chlorite (aqueous). Treatments with resting cells of *S. oneidensis* MR-1 in the presence and absence of AQDS are shown in relation to abiotic controls. The error bars represent the standard error of triplicate measurements.

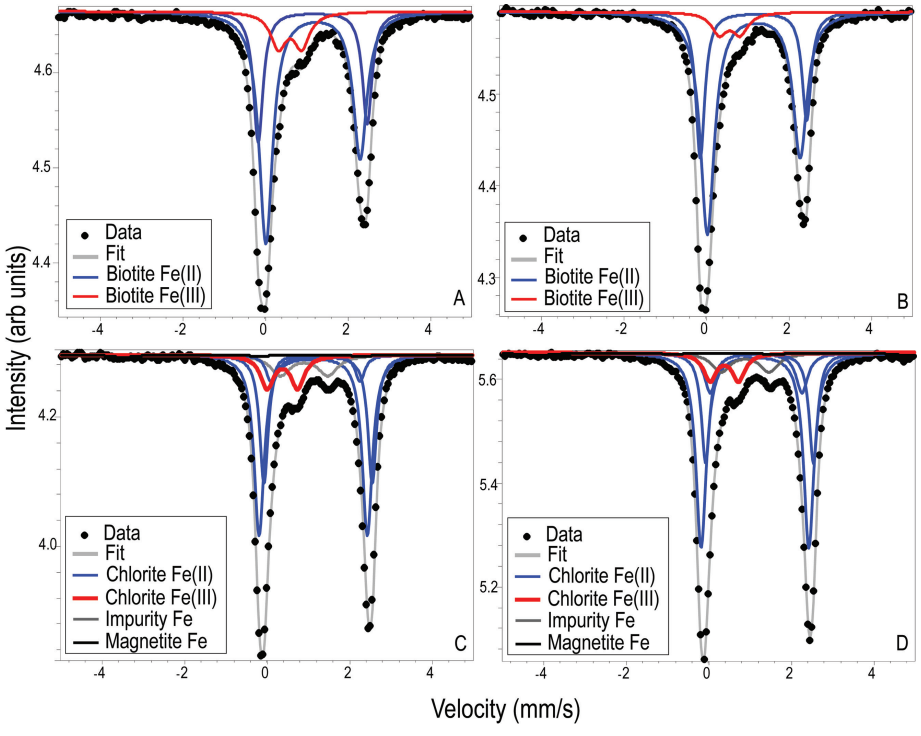

FIGURE 2. Mössbauer spectra for iron in: (**a**) unaltered biotite; (**b**) bioreduced biotite; (**c**) unaltered chlorite; and (**d**) bioreduced chlorite. Note the decrease in the shoulder feature attributable to Fe(III) after microbial reduction.

attributable to the Fe(III) present (Fig. 2). The spectra were fitted with doublets arising from two octahedral Fe(II) sites corresponding to the two sites in the octahedral layer of phyllosilicates, and present in a 2:1 ratio. Those are the M1 site (where hydroxyl groups are in *trans* configuration) and M2 site (with hydroxyl groups in *cis* coordination) with M2 being the more abundant. The Fe(III) contribution was associated with a single unresolved Fe(III) octahedral site doublet (see Table 2). An asymmetry in the intensities of the two Fe(II) doublets of the spectrum was attributed to preferential orientation of the biotite grains within the prepared sample, and has been fitted with asymmetric doublets. This provided a good fit to the experimental data ($\chi^2 = 2.64$ and 1.35 for the unaltered and bioreduced (+AQDS) samples, respectively). There was no detectable Fe(III) in tetrahedral coordination in the biotite.

The chlorite spectrum also contains the prominent doublet characteristic of Fe(II) and the shoulder associated with Fe(III) (Fig. 2) as in previously published chlorite spectra (Smyth et al. 1997). The data were fitted with three doublets attributable to Fe(II) in octahedral sites: two in the octahedral sheet (M1, M2), and one in the brucite-like interlayer (site 3). A single doublet attributable to Fe(III) in octahedral sites was also fitted. A second shoulder seen on the Fe(II) doublet at a higher velocity, was similar to a feature observed in a published chlorite spectrum interpreted as being from Fe(II) in tetrahedral coordination (Gregori and Mercader 1994). However, this is a very unlikely coordination for Fe(II). The shoulder may be due to an impurity, but is not due to ilmenite (Dyar et al. 2006) or garnet. Our spectra also display a very weak sextet, indicating a minor component from a magnetically ordered iron species, consistent with magnetite. Although the room-temperature spectra of magnetite require fitting with two partly overlapping sextets arising from iron in tetrahedral and octahedral sites, the quality of the data obtained here mean that we can only report an average value for these combined sextets.

Based on the relative areas of the fitted doublets, Fe(III) accounted for approximately 12.6% of the total Fe in biotite, and 10.4% in chlorite. These spectra showed that microbial reduction of the minerals led to a decrease in the intensity of the doublet attributable to Fe(III) for both minerals, indicating that the bulk Fe speciation was affected by the microbial activity. The difference between the unaltered and bioreduced minerals was small overall; however, this result was highly reproducible. Using data reported in this paper and two independent preliminary experiments, there was a statistically significant difference between the average of the Fe(III) in the unaltered minerals compared to the average of the Fe(III) in the bioreduced minerals at the 1% level (this indicates that there is 99% chance that the result reflects a true difference between the averages. The percentage Fe(III) of the total iron after reduction was approximately 8% in both minerals, a decrease of approximately 36% of the starting Fe(III) amount in biotite, and 21% in chlorite. In biotite, the decrease in Fe(III) was associated with an increase of Fe(II) in the more abundant Fe-site, interpreted as the M2 *cis* site based on the mineral structure. This suggests that the transformation of Fe(III) to Fe(II) within the bulk of the mineral occurs predominantly at the M2 sites. The small change in relative abundance of Fe(II) in the M1 sites may be because most of those sites were already occupied by Fe(II), as can also be inferred from theoretical calculations indicating that the M1 sites may act as electron traps (Rosso and Ilton 2003).

Effect of bioreduction on the mineral structure

No large-scale changes in the structures of the minerals were seen in the XRD patterns of the bioreduced minerals and no new secondary minerals were detected (XRD patterns are shown in Supplementary Figs. 1 and 2[1]). There was a slight increase in the surface area of biotite after bioreduction from 9.02 to 10.65 m^2/g, although results for biotite could be influenced by the grains clumping together due to static charge. There was no change in the surface area of the chlorite after bioreduction (6.15 m^2/g).

To investigate further the effect of bioreduction on the stability of the minerals, a 0.1 mL aliquot of mineral-solution slurry from each microbial reduction experiment was suspended in 0.5 M HCl for 1 h. A subsample of the supernatant was analyzed by ICP-AES for cations that were released from the modified mineral structure after reduction (Fig. 3). This operationally defined extraction allowed an assessment of the effect of reduction on mineral stability.

In biotite, the amount of Si that is dissolved can be used as a guide to the dissolution rate of material in the tetrahedral layer, and the amount of Mg for the dissolution of the octahedral layer (Hopf et al. 2009). The dissolution of the biotite by 0.5 M HCl led to non-stoichiometric release of cations (Acker and Bricker 1992; Hamer et al. 2003). Based on the solid-to-solution ratio used in these experiments, there were 56 mmol of biotite and 37 mmol of chlorite per liter. The dissolution of the silicate tetrahedral layer by the weak acid was calculated as being 4.7–7.0%

TABLE 2. Mössbauer parameters for biotite and chlorite

	Isomer shift[a] (mm/s)	Quadropole splitting[a] (mm/s)	Hyperfine field[a] (kOe)	Area (%) in unaltered mineral	Area (%) after bioreduction
Biotite					
Fe(II)(M1)	1.151	2.639		27.2	28.4
Fe(II)(M2)	1.158	2.281		60.2	63.5
Fe(III)	0.602	0.562		12.6	8.1
Chlorite					
Fe(II)(site 1)	1.239	2.621		26.2	21.3
Fe(II)(site 2)	1.121	2.620		43.7	46.2
Fe(II)(site 3)	1.173	2.162		6.1	10.8
Fe(III)	0.375	0.738		10.4	8.2
Impurity	0.898	1.150		9.4	7.9
Magnetite[b]	0.670	–0.38	482	4.2	5.6

[a] The parameter values are those for the unaltered sample. They varied by <1% from those in the bioreduced sample.
[b] Values reported for magnetite are an average for the combined sextets.

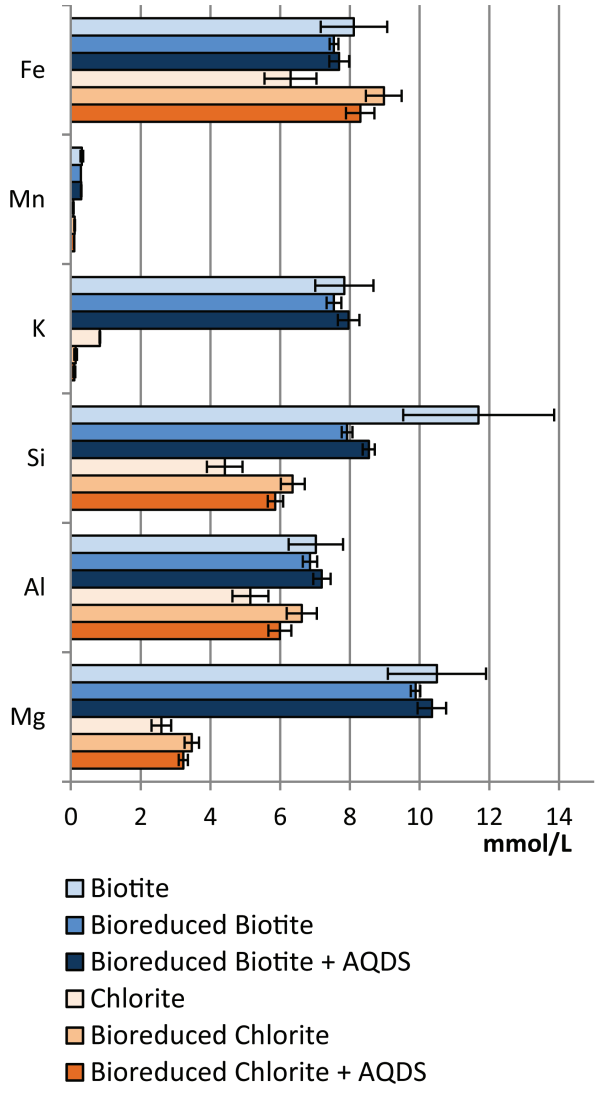

FIGURE 3. Concentrations of cations in acid extractions of unaltered and bioreduced minerals. Error bars show the standard error of triplicate measurements.

of the available Si. On the other hand, as much as 15.0–15.8% of the interlayer K from the biotite was lost during the weak acid extraction, probably due to exchange with H^+. Al was preferentially dissolved (12.5–13.1%) compared to Si, possibly relating to the lower activation energy of sites occupied by this element (Malmström and Banwart 1997) or destabilization of Al-substituted sites in the tetrahedral sheet. Loss of Fe was almost stoichiometric with that of Mg (11.7–12.4% and 12.2–13.2%, respectively) suggesting that, in the biotite, dissolution of the octahedral sheet was congruent. Interestingly, Mn was preferentially extracted compared to Mg (17.2–18.6%). The concentration of dissolved Mg was approximately twice that of Si, suggesting that the octahedral layer was more susceptible to dissolution than the Si-tetrahedral layer in all treatments. However there was no significant difference between the HCl-extractable cation profile of unaltered compared to bioreduced biotite, indicating that bioreduction in this mineral does not significantly affect its overall stability.

Dissolution of chlorite was also incongruent (Brandt et al. 2003). The pattern in the chlorite was similar to that of biotite, but the differences in relative release were less pronounced. Here, preferential loss of Mn (9.3–14.7%) occurred, presumably by similar processes to those in biotite. The difference between the loss of the octahedrally coordinated cations Mg (7.2–10.1%) and Fe (4.6–6.6%) and the tetrahedral Si (4.6–6.6%) was less than in biotite suggesting that the octahedral sheet in chlorite is more stable to acid dissolution than that in biotite. Interestingly, in contrast to the biotite, there was a notable difference in the acid-extractable cation concentration in chlorite between the different treatments. Greater concentrations of all cations were detected in the extractions from the microbially reduced chlorite samples compared to the abiotic samples, indicating that microbial reduction of this mineral may make it more susceptible to dissolution and that bioreduction destabilises the whole structure.

Reduction of biotite and microbial growth

The physical relationship between the bacteria and minerals was studied using imaging techniques. Bacteria were seen attached to mineral surfaces in all experiments. Images obtained by ESEM from treatments with washed resting cells of *S. oneidensis* MR-1 (see Fig. 4), show oval shapes approximately 1–2

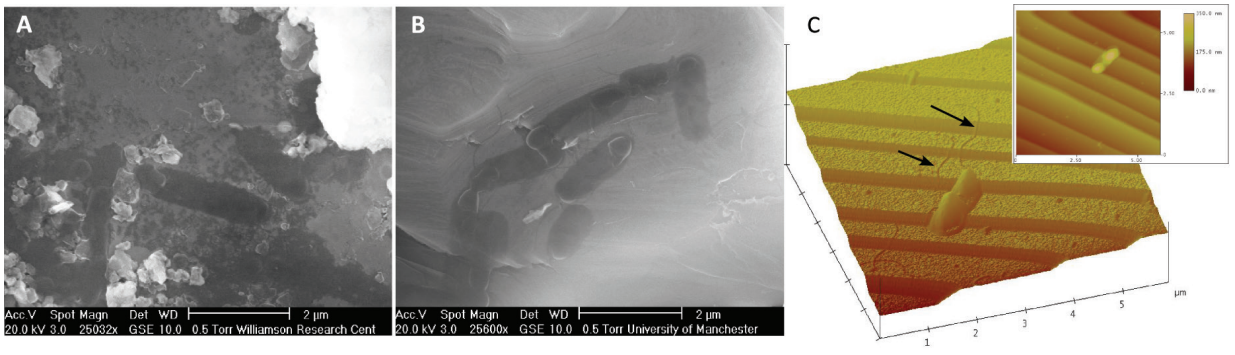

FIGURE 4. Mineral surfaces in experiments with washed cell suspensions of *S. oneidensis* MR-1 in bicarbonate buffer amended with 10 mM lactate. ESEM images of biotite (**a**) and chlorite (**b**) after bioreduction. AFM height image of a biotite flake after bioreduction (**c**) and 3D representation of the height data (inset) show a stepped biotite edge and an attached cell.

μm long (approximate size of the cells), distributed randomly over the surface of the biotite flakes.

There was no clustering of these oval-shaped features at particular regions of the surface such as steps, suggesting that the ability of *S. oneidensis* MR-1 to reduce the mineral was not predicated on the bacteria being located near points of access to the octahedral layer.

Mineral flakes were also imaged using AFM. Here, bacteria were seen clearly on the mineral surface. AFM images showed *S. oneidensis* MR-1 cells had two or more appendages with an approximate thickness of 5–7 nm. These appendages may be dehydrated flagella, but the dimensions are also similar to those of the pili *S. oneidensis* MR-1 can produce for attachment to mineral surfaces (Bouhenni et al. 2010). They may also play a role in electron transfer, as has been shown for similar-sized "nanowires" produced by this bacterium (Gorby et al. 2006).

Fluorescence microscopy images of the bacteria on the biotite flakes were used to estimate the increase in biomass in growing-cell experiments, in which biotite was added to fully defined medium lacking other electron acceptors [i.e., Fe(III) associated with the biotite was the only available electron acceptor]. In the early stages of the experiment (two weeks), increase in biomass was observed predominantly as an increase in the number of discrete bacteria at mineral surfaces in growth treatments. Under growth conditions, higher bacterial densities were visible along some structural irregularities, e.g., biotite steps parallel to the 001 layer (see Supplementary Fig. 3[1]). Despite differences in samples from each experiment due, for example, to mineral heterogeneity, the average cell numbers per grid square in growth treatments (6.9 ± 1.9 and 6.3 ± 1.4) were significantly higher than those in no-donor treatments (2.6 ± 0.6, see Fig. 5). No cells were observed in non-inoculated controls.

Four weeks after the start of the experiment, the cell numbers were also greater in the growth treatments (where electron donor had been added) (7.9 ± 2.4 and 5.3 ± 1.9) than in the no-donor treatments (1.3 ± 0.4). The number of discrete bacteria was lower than that in the corresponding treatments at two weeks while the number of micro-colonies had increased. A micro-colony was defined as a cluster of more than 10 cells and forming a continuous cover over the biotite surface. This trend toward concentration of biomass in colonies was seen to continue to eight weeks, by which time most areas were covered with numerous colonies, in some cases formed by fusing together smaller colonies with the number of single cells decreasing even further. The cell number estimates at eight weeks show that under growth conditions, overall biomass, expressed as approximate cell numbers, had increased further (7.6 ± 2.0 and 7.3 ± 1.0) and cell numbers in the no-donor control had continued to decrease (1.0 ± 0.5). This suggests a growth progression from survival of the added cells and some division (leading to discrete cells visible after two weeks), to concentration of growth in certain locations where colonies started to form after two weeks of growth (Zhang et al. 2010). Progressively fewer single cells were visible in areas free of colonies in the later stages of the experiment, suggesting that after four weeks, survival of cells away from colonies may have been limited. This is also supported by the observed decrease in cell numbers in the no-donor controls, possibly reflecting cell death and degradation after 2–4 weeks. By contrast, cell division in colonies in the growth experiments led to formation of new cells that were then visible as parts of these colonies at four and eight weeks. Similar colony progression of *S. oneidensis* MR-1 has been observed by Thormann et al. (2004) in flow-through experiments and was shown to be associated with strong attachment of the colony to the substrate surface.

The significant increase in cell numbers and the increase in the number of micro-colonies in experiments with bacteria in growth medium compared to the abiotic controls indicate that *S. oneidensis* MR-1 was able to conserve energy for growth from the reduction of structural Fe(III) within biotite.

Discussion

Method of microbial reduction of biotite and chlorite

The results presented here show that bacteria can mediate the reduction of Fe(III) in biotite and chlorite, and that this reaction affects both the acid-extractable and structural iron within the minerals. The rates of reduction were similar to those reported for the bioreduction of chlorite by *Shewanella putrefaciens* CN32 by Bishop et al. (2011). The overall extent of reduction of chlorite reported here was lower than indicated by these authors, likely relating to the greater particle size used. There was

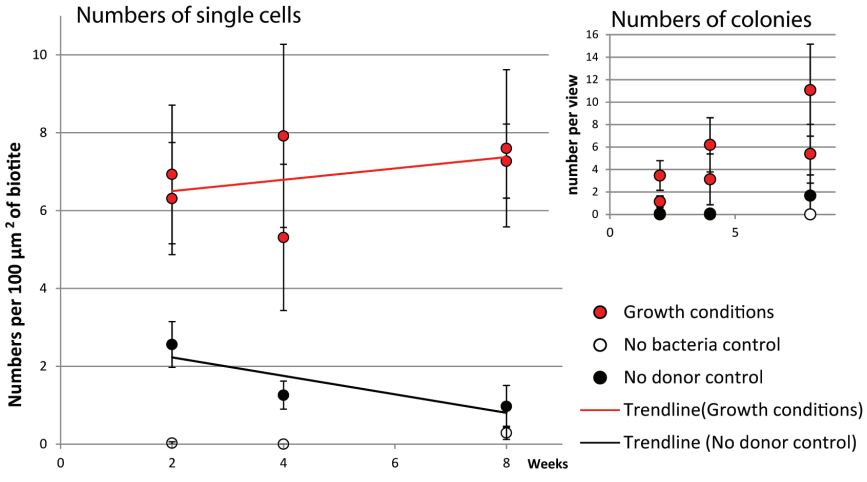

◀**Figure 5.** Cell counts in growth experiments compared to abiotic and no-donor controls. Main figure shows counts of individual cells per grid square (each point represents the average of 300 measurements per experiment) including linear trendlines of the results of the growth experiments and no donor controls. Inset figure shows the number of colonies visible in a field of view for the same experiments (average of 15 measurements per experiment). Error bars represent the combined standard deviation, reflecting the three levels of variability in the counts (grid square, view area, and flake).

no significant difference in the integrity of the minerals after bioreduction (when compared to non-inoculated controls); no features were observed that could be attributed to dissolution of the mineral by microbial activity, such as etch pits, or roughening of the mineral surface as seen in long-term experiments with fungi (Balogh-Brunstad et al. 2008; Kapitulcinova et al. 2008), or formation of secondary minerals. This is consistent with the chemical data, which suggest that microbially mediated mineral reduction is predominantly a solid-state reaction.

There was also no effect of microbial reduction on the stability of biotite when exposed to acid dissolution. This may be due to the layers of linked SiO_4 tetrahedra stabilizing the overall mineral structure. In contrast, bioreduced chlorite was more susceptible to acid dissolution than unaltered chlorite, suggesting that its structure is more destabilized by microbial reduction than is that of biotite, despite greater and more unequal loss of cations from the biotite. In chlorite, the reductive transformation of Fe(III) to Fe(II) in the tetrahedral-octahedral-tetrahedral layer may compromise the integrity of the overall mineral by causing greater destabilization of the brucite interlayer. In biotite, the ratio of release of the octahedral cations Mg:Fe by acid dissolution was slightly less than one, whereas in chlorite it was greater than one. This suggests that, whereas in biotite loss of cations from the octahedral layer was almost stoichiometric, in chlorite there was a relatively enhanced release of Mg. This suggests enhanced instability of the brucite-like interlayer in chlorite, which is likely to have a greater Mg:Fe ratio than the 2:1 unit octahedral layer.

Mechanism of reduction

Several studies have shown that Fe(III) within phyllosilicates is available for microbial reduction (Bishop et al. 2011; Dong et al. 2009; Jaisi et al. 2007; Kostka et al. 1996; Stucki 2011). However, the mechanism of this solid-state reduction remains elusive. The electrical conductivity properties of such minerals suggest the likely pathways of electron transfer through them. For biotite, greatest conductivity has been recorded parallel to the mineral cleavage [along the (001) surface] and is two to five orders of magnitude greater than the conductivity recorded perpendicular to basal planes (along the "z" mineral axis; Ruscher and Gall 1995). Their results suggested that in biotite (and also in chlorite) electrons travel most readily two-dimensionally through octahedral layers. In our experiments, we observed greater microbial biomass growing along mineral surface features interpreted as edges and steps in biotite (see Supplementary Figure 3[1]), indicating greater availability of energy for growth at sites where the octahedral layer is directly accessible.

There was almost complete conversion of Fe(III) to Fe(II) near the mineral surface (suggested by the weak acid extractable ferrozine results, see Figs. 1a and 1b) and incomplete reduction of the bulk Fe(III) (see Fig. 2, Table 2), consistent with an interpretation of enhanced reduction near to the location of microbial activity. Our results suggest that reduction of the bulk mineral may occur through electron transfer from the site of reduction (an area of higher electron density) to more "distal" Fe(III) sites (Wilkins et al. 2007). This transfer would effectively regenerate the Fe(III) near the mineral surface for further reduction, while increasing the zone of the microbial reduction. A similar "reduction front" advancing from the mineral surface to the center of mineral grains was suggested for the microbial reduction of nontronite (Ribeiro et al. 2009) and may prevail in microbial reduction of sheet silicates.

Implications

Previous studies have demonstrated the ability of *S. oneidensis* MR-1 to respire and grow using Fe(III) in iron oxides (Roden and Zachara 1996) or smectite (Kostka et al. 2002) as the sole electron acceptors. However, to our knowledge, this is the first study to demonstrate the ability of this bacterium to reduce structural Fe(III) in biotite and conserve energy from this reduction. The proposed mechanism of microbial reduction of sheet silicates creates a framework for further research into the bioavailability of mineral Fe(III), and to elucidate pathways of contaminant immobilization by these minerals. This work has important implications for our understanding of microbial metabolism and ecology in biotite-dominated horizons such as granite rock environments or phyllosilicate-rich soils, and the role of these minerals in contaminant dynamics.

Acknowledgments

We gratefully acknowledge funding from EPSRC Grant (EP/G063699/1) as part of the BANDD consortium (Biogeochemical Applications in Nuclear Decommissioning and Waste Disposal). We thank Paul Wincott for help with the Mössbauer analysis and AFM imaging and Paul Lythgoe for ICP-AES analysis. We would also like to thank Thelma Berquo, Hailiang Dong, and John Zachara for their helpful suggestions for improvement of this manuscript.

References cited

Acker, J.G., and Bricker, O.P. (1992) The influence of pH on biotite dissolution and alteration kinetics at low temperature. Geochimica et Cosmochimica Acta, 56, 3073–3092.

Baik, M.H., Kim, S.S., Lee, J.K., Lee, S.Y., Kim, G.Y., and Yun, S.T. (2010) Sorption of C-14, Tc-99, Cs-137, Sr-90, Ni-63, and Am-241 onto a rock and a fracture-filling material from the Wolsong low- and intermediate-level radioactive waste repository, Gyeongju, Korea. Journal of Radioanalytical and Nuclear Chemistry, 283, 337–345.

Balogh-Brunstad, Z., Keller, C.K., Dickinson, J.T., Stevens, F., Li, C.Y., and Bormann, B.T. (2008) Biotite weathering and nutrient uptake by ectomycorrhizal fungus, Suillus tomentosus, in liquid-culture experiments. Geochimica et Cosmochimica Acta, 72, 2601–2618.

Barker, W.W., and Banfield, J.F. (1996) Biologically versus inorganically mediated weathering reactions: Relationships between minerals and extracellular microbial polymers in lithobiontic communities. Chemical Geology, 132, 55–69.

Barker, W.W., Welch, S.A., Chu, S., and Banfield, J.F. (1998) Experimental observations of the effects of bacteria on aluminosilicate weathering. American Mineralogist, 83, 1551–1563.

Bishop, M.E., Dong, H.L., Kukkadapu, R.K., Liu, C.X., and Edelmann, R.E. (2011) Bioreduction of Fe-bearing clay minerals and their reactivity toward pertechnetate (Tc-99). Geochimica et Cosmochimica Acta, 75, 5229–5246.

Bouhenni, R.A., Vora, G.J., Biffinger, J.C., Shirodkar, S., Brockman, K., Ray, R., Wu, P., Johnson, B.J., Biddle, E.M., Marshall, M.J., and others. (2010) The role of *Shewanella oneidensis* MR-1 outer surface structures in extracellular electron transfer. Electroanalysis, 22, 856–864.

Brandt, F., Bosbach, D., Krawczyk-Bärsch, E., Arnold, T., and Bernhard, G. (2003) Chlorite dissolution in the acid pH-range: a combined microscopic and macroscopic approach. Geochimica et Cosmochimica Acta, 67, 1451–1461.

Cutting, R.S., Coker, V.S., Fellowes, J.W., Lloyd, J.R., and Vaughan, D.J. (2009) Mineralogical and morphological constraints on the reduction of Fe(III) minerals by *Geobacter sulfurreducens*. Geochimica et Cosmochimica Acta, 73, 4004–4022.

Dong, H.L. (2012) Clay-microbe interactions and implications for environmental mitigation. Elements, 8, 113–118.

Dong, H.L., Kostka, J.E., and Kim, J. (2003a) Microscopic evidence for microbial dissolution of smectite. Clays and Clay Minerals, 51, 502–512.

Dong, H.L., Kukkadapu, R.K., Fredrickson, J.K., Zachara, J.M., Kennedy, D.W., and Kostandarithes, H.M. (2003b) Microbial reduction of structural Fe(III) in illite and goethite. Environmental Science and Technology, 37, 1268–1276.

Dong, H.L., Jaisi, D.P., Kim, J., and Zhang, G.X. (2009) Microbe-clay mineral interactions. American Mineralogist, 94, 1505–1519.

Dyar, M.D. (1993) Mössbauer spectroscopy of tetrahedral Fe^{3+} in trioctahedral

micas—Discussion. American Mineralogist, 78, 665–668.
Dyar, M.D., Agresti, D.G., Schaefer, M.W., Grant, C.A., and Sklute, E.C. (2006) Mössbauer spectroscopy of earth and planetary materials. Annual Review of Earth and Planetary Sciences, vol. 34, p. 83–125. Annual Reviews, Palo Alto.
Eggleton, R.A., and Banfield, J.F. (1985) The alteration of granitic biotite to chlorite. American Mineralogist, 70, 902–910.
Gorby, Y.A., Yanina, S., McLean, J.S., Rosso, K.M., Moyles, D., Dohnalkova, A., Beveridge, T.J., Chang, I.S., Kim, B.H., Kim, K.S., and others. (2006) Electrically conductive bacterial nanowires produced by *Shewanella oneidensis* strain MR-1 and other microorganisms. Proceedings of the National Academy of Sciences, 103, 11358–11363.
Gregori, D.A., and Mercader, R.C. (1994) Mössbauer study of some Argentinian chlorites. Hyperfine Interactions, 83, 495–498.
Hamer, M., Graham, R.C., Amrheim, C., and Bozhilov, K.N. (2003) Dissolution of ripidolite (Mg, Fe-chlorite) in organic and inorganic acid solutions. Soil Science Society of America Journal, 67, 654–661.
Hopf, J., Langenhorst, F., Pollok, K., Merten, D., and Kothe, E. (2009) Influence of microorganisms on biotite dissolution: An experimental approach. Chemie der Erde-Geochemistry, 69, 45–56.
Jaisi, D.P., Kukkadapu, R.K., Eberl, D.D., and Dong, H.L. (2005) Control of Fe(III) site occupancy on the rate and extent of microbial reduction of Fe(III) in nontronite. Geochimica et Cosmochimica Acta, 69, 5429–5440.
Jaisi, D.P., Dong, H.L., and Liu, C.X. (2007) Influence of biogenic Fe(II) on the extent of microbial reduction of Fe(III) in clay minerals nontronite, illite, and chlorite. Geochimica et Cosmochimica Acta, 71, 1145–1158.
Jaisi, D.P., Eberl, D.D., Dong, H.L., and Kim, J. (2011) The formation of illite from nontronite by mesophilic and thermophilic bacterail reaction. Clays and Clay Minerals, 59, 21–33.
Kameda, J., Sugimori, H., and Murakami, T. (2009) Modification to the crystal structure of chlorite during early stages of its dissolution. Physics and Chemistry of Minerals, 36, 537–544.
Kapitulcinova, D., Cockell, C.S., Hallam, K.R., and Ragnarsdottir, K.V. (2008) Effect of cyanobacterial growth on biotite surfaces under laboratory nutrient-limited conditions. Mineralogical Magazine, 72, 71–75.
Kim, J., Dong, H.L., Seabaugh, J., Newell, S.W., and Eberl, D.D. (2004) Role of microbes in the smectite-to-illite reaction. Science, 303, 830–832.
Kostka, J.E., Stucki, J.W., Nealson, K.H., and Wu, J. (1996) Reduction of structural Fe(III) in smectite by a pure culture of *Shewanella putrefaciens* strain MR-1. Clays and Clay Minerals, 44, 522–529.
Kostka, J.E., Wu, J., Nealson, K.H., and Stucki, J.W. (1999) The impact of structural Fe(III) reduction by bacteria on the surface chemistry of smectite clay minerals. Geochimica et Cosmochimica Acta, 63, 3705–3713.
Kostka, J.E., Dalton, D.D., Skelton, H., Dollhopf, S., and Stucki, J.W. (2002) Growth of iron(III)-reducing bacteria on clay minerals as the sole electron acceptor and comparison of growth yields on a variety of oxidized iron forms. Applied and Environmental Microbiology, 68, 6256–6262.
Krawczyk-Barsch, E., Arnold, T., Reuther, H., Brandt, F., Bosbach, D., and Bernhard, G. (2004) Formation of secondary Fe-oxyhydroxide phases during the dissolution of chlorite effects on uranium sorption. Applied Geochemistry, 19, 1403–1412.
Lovley, D.R., and Phillips, E.J.P. (1987) Rapid assay for microbially reducible ferric iron in aquatic sediments. Applied and Environmental Microbiology, 53, 1536–1540.
——— (1988) Novel mode of microbial energy-metabolism–organic-carbon oxidation coupled to dissimilatory reduction of iron or manganese. Applied and Environmental Microbiology, 54, 1472–1480.
Malmström, M., and Banwart, S. (1997) Biotite dissolution at 25°C: The pH dependence of dissolution rate and stoichiometry. Geochimica et Cosmochimica Acta, 61, 2779–2799.
McKinley, J.P., Zeissler, C.J., Zachara, J.M., Serne, R.J., Lindstrom, R.M., Schaef, H.T., and Orr, R.D. (2001) Distribution and retention of Cs-137 in sediments at the Hanford Site, Washington. Environmental Science and Technology, 35, 3433–3441.
Rancourt, D.G., Dang, M.Z., and Lalonde, A.E. (1992) Mossbauer spectroscopy of tetrahedral Fe^{3+} in trioctahedral micas. American Mineralogist, 77, 34–43.
Ribeiro, F.R., Fabris, J.D., Kostka, J.E., Komadel, P., and Stucki, J.W. (2009) Comparisons of structural iron reduction in smectites by bacteria and dithionite: II. A variable-temperature Mossbauer spectroscopic study of Garfield nontronite. Pure and Applied Chemistry, 81, 1499–1509.
Roden, E.E., and Urrutia, M.M. (2002) Influence of biogenic Fe(II) on bacterial crystalline Fe(III) oxide reduction. Geomicrobiology Journal, 19, 209–251.
Roden, E.E., and Zachara, J.M. (1996) Microbial reduction of crystalline iron(III) oxides: Influence of oxide surface area and potential for cell growth. Environmental Science and Technology, 30, 1618–1628.
Rosso, K.M., and Ilton, E.S. (2003) Charge transport in micas: The kinetics of Fe-II/III electron transfer in the octahedral sheet. Journal of Chemical Physics, 119, 9207–9218.
Ruscher, C.H., and Gall, S. (1995) On the polaron mechanism in iron-bearing trioctahedral phyllosilicates—an investigation of the electrical and optical properties. Physics and Chemistry of Minerals, 22, 468–478.
Seabaugh, J.L., Dong, H.L., Kukkadapu, R.K., Eberl, D.D., Morton, J.P., and Kim, J. (2006) Microbial reduction of Fe(III) in the Fithian and Muloorina illites: Contrasting extents and rates of bioreduction. Clays and Clay Minerals, 54, 67–79.
Smyth, J.R., Dyar, M.D., May, H.M., Bricker, O.P., and Acker, J.G. (1997) Crystal structure refinement and Mossbauer spectroscopy of an ordered, triclinic clinochlore. Clays and Clay Minerals, 45, 544–550.
Stucki, J.W. (2011) A review of the effects of iron redox cycles on smectite properties. Comptes Rendus Geoscience, 343, 199–209.
Stucki, J.W., Golden, D.C., and Roth, C.B. (1984) Effects of reduction and reoxidation of structural iron on the surface charge and dissolution of dioctahedral smectites. Clays and Clay Minerals, 32, 350–356.
Thormann, K.M., Saville, R.M., Shukla, S., Pelletier, D.A., and Spormann, A.M. (2004) Initial phases of biofilm formation in *Shewanella oneidensis* MR-1. Journal of Bacteriology, 186, 8096–8104.
von Canstein, H., Ogawa, J., Shimizu, S., and Lloyd, J.R. (2008) Secretion of flavins by *Shewanella* species and their role in extracellular electron transfer. Applied and Environmental Microbiology, 74, 615–623.
Wilkins, M.J., Wincott, P.L., Vaughan, D.J., Livens, F.R., and Lloyd, J.R. (2007) Growth of *Geobacter sulfurreducens* on poorly crystalline Fe(III) oxyhydroxide coatings. Geomicrobiology Journal, 24, 199–204.
Zhang, M.N., Ginn, B.R., Dichristina, T.J., and Stack, A.G. (2010) Adhesion of *Shewanella oneidensis* MR-1 to iron (oxy)(hydr)oxides: Microcolony formation and isotherm. Environmental Science and Technology, 44, 1602–1609.
Zhang, G.X., Burgos, W.D., Senko, J.M., Bishop, M.E., Dong, H.L., Boyanov, M.I., and Kemner, K.M. (2011) Microbial reduction of chlorite and uranium followed by air oxidation. Chemical Geology, 283, 242–250.

Manuscript received October 16, 2013
Manuscript accepted February 17, 2014
Manuscript handled by Joshua Feinberg